Human umbilical cord blood mononuclear cells laden hydrogels made from carboxymethyl chitosan and oxidized hyaluronic acid for wound healing

Shaowen Kong, Jie Song, Yuandou Wang, Shuxin Wang, Feng Su, Suming Li

Human umbilical cord blood mononuclear cells laden hydrogels made from carboxymethyl chitosan and oxidized hyaluronic acid for wound healing

Shaowen Kong[1] | **Jie Song**[1] | **Yuandou Wang**[1] | **Shuxin Wang**[1] | **Feng Su**[1,2] | **Suming Li**[3]

[1]College of Chemical Engineering, Qingdao University of Science and Technology, Qingdao, China

[2]Institute of High Performance Polymers, Qingdao University of Science and Technology, Qingdao, China

[3]Institut Européen des Membranes, IEM UMR 5635, Université Montpellier, CNRS, ENSCM, Montpellier, France

Correspondence
Feng Su, College of Chemical Engineering, Qingdao University of Science and Technology, Qingdao 266042, China.
Email: sufeng@qust.edu.cn

Suming Li, Institut Européen des Membranes, IEM UMR 5635, Université Montpellier, CNRS, ENSCM, Montpellier, France.
Email: suming.li@umontpellier.fr

Funding information
Natural Science Foundation of Shandong Province, Grant/Award Number: ZR2021ME208; Wanhua Chemical Group, Grant/Award Number: 20213702032181

Abstract

A dynamic hydrogel was prepared from *N*,*O*-carboxymethyl chitosan (NOCC) and oxidized aldehyde-containing hyaluronic acid (A-HA) by Schiff base reaction. The resulted NOCC/A-HA hydrogels were characterized by Fourier transform infrared spectroscopy and scanning electron microscopy (SEM). The rheological, swelling, and self-healing properties of hydrogels were determined. The hydrogels present interconnected porous structure, high swelling rate, and outstanding self-healing capacity. The biocompatibility of hydrogels was evidenced by MTT assay and zebrafish embryonic toxicity test. Human umbilical cord blood mononuclear cells (CB-MNC) were encapsulated in the hydrogel. High cell viability above 50% was obtained after 21 days culture. A mouse scald model was realized to evaluate the potential of cell laden hydrogel in wound healing. Compared to the control group and the hydrogel group, the cell laden hydrogel group exhibits faster epidermal regeneration, reduced inflammation and more neovascularization. Therefore, NOCC/A-HA hydrogels encapsulating CB-MNC could be a promising therapy in the treatment of burns or scalds.

KEYWORDS

burns, carboxymethyl chitosan, dynamic hydrogel, human umbilical cord blood mononuclear cells, hyaluronic acid, wound dressing

1 | INTRODUCTION

Burns and scalds are damages to the skin caused by heat. The healing of skin burns and scalds could be a long and complex process depending on the degree of damage.[1] Dressings such as gauze, bandages, and skin grafts are currently used in clinics to treat these wounds.[2] Scarring could occur after wound healing, causing severe psychological stress to patients.[3] As a moist environment is beneficial to wound healing, a variety of novel dressings have been developed, including hydrogels, foams, and film dressings.[4]

Hydrogels are composed of hydrophilic polymers involved in a three-dimensional network by physical or chemical crosslinking.[5] It has been shown that burns treated with hydrogel dressings healed faster than burns treated with usual dressings.[6] Hydrogels are capable of absorbing huge amounts of water without dissolving.[7] Due to their excellent moisturizing capacity, hydrogels can keep the wound moist and play an active role in epidermal regeneration and removal of necrotic tissue.[8] Wound healing can be monitored with overlying dressings, as hydrogels are usually transparent.[9] In addition,

the degradation rate of hydrogels can be adjusted by varying the composition, crosslinking route and crosslinking density, and so forth.[10] These properties make hydrogels a material of choice for wound healing applications.[11]

Chitosan, a polysaccharide obtained by deacetylation of chitin, has been widely studied for the development of novel hydrogels in the past decades due to their outstanding biocompatibility, biodegradability, low toxicity, and antibacterial activity.[12–15] Chitosan is soluble only in acidic media due to strong intra- and intermolecular hydrogen bonding.[16] In contrast, the derivative of chitosan, *N*,*O*-carboxymethyl chitosan (NOCC) is readily soluble in water at neutral pH.[17] NOCC is obtained by introduction of carboxymethyl group at the N and/or O positions of D-glucosamine.[18] It is widely used to prepare in situ dynamic hydrogels by Schiff base reaction with formation of reversible imine bonds between its amino groups with aldehyde-containing species.[19–22]

Hyaluronic acid (HA) is a glycosaminoglycane present in the human body as the major component of extra cellular matrix (ECM).[23] It has been reported that 3D ECM gels can promote the growth of stem cells.[24] HA based hydrogels attracted much interest for applications in drug delivery, wound healing and tissue engineering due to their outstanding biocompatibility and biodegradability.[25–27] The oxidation of HA generates aldehyde-containing HA (A-HA) whose aldehyde groups can react with amino groups to form hydrogels by Schiff base reaction.[28] The resulted dynamic hydrogels were used for postoperative adhesion prevention, abdominal tissue repair, or wound dressing.[29]

Human umbilical cord blood mononuclear cells (CB-MNC) contain a large number of immature immune cells, hematopoietic stem cells and progenitor cells.[30] Among them, stem cells and progenitor cells have multidirectional differentiation potential.[31,32] Athanassopoulos et al. induced CB-MNC to generate endothelial colony-forming cells (ECFC) and demonstrated their ability to form a vascular network, which can be used as a dermal substitute in clinics for repairing scald wounds.[33] Chang et al. evaluated the cell therapy efficacy of CB-MNC combined with HA hydrogel in a pig myocardial infarction model. Data showed that CB-MNC alone or combined with HA hydrogel significantly decreased the scar area and promoted angiogenesis in the infarcted region.[34] In a mouse model mimicking hallmarks of bronchopulmonary dysplasia (BPD), Chen et al. observed that CB-MNC are efficient in alleviating BPD as cell infusion allows to prevent alveolar simplification and pulmonary vascular loss, to restore pulmonary respiratory function and to balance the inflammatory response.[35] Boissel et al. reported that CB-MNC enhance the expansion of cord blood natural killer (NK) cells, and suggested that CB-MNC could enrich NK cell progenitors and can be used for immunotherapy.[36] On the other hand, wound treatments using stem cells are generally performed by injection. But cell migration can occur due to skin pressure, which affects the clinical application of stem cells.[37] Combination of hydrogels and mesenchymal stem cells could significantly promote wound healing and tissue remodeling, and reduce inflammatory responses.[38] Nevertheless, combination of CB-MNC and hydrogels has not been investigated for applications as wound dressing, so far.

The aim of the present study was to evaluate the potential of CB-MNC laden dynamic hydrogels in the treatment of burns or scalds, as shown in Scheme 1. Hydrogels were prepared from NOCC and A-HA through Schiff base reaction under mild conditions. The rheological and self-healing properties of hydrogels were studied by using various analytical techniques. The biocompatibility of hydrogels was evaluated by MTT assay and zebrafish toxicity test. A mouse scald model was used to evaluate the effect of CB-MNC loaded hydrogels on wound healing. The hydrogels could serve as a cell scaffold and provide a wet environment for wound healing, and the stem cells could play an active role to promote scald wound healing and to reduce scar formation.

2 | MATERIALS AND METHODS

2.1 | Materials and reagents

L929 mouse fibroblasts were purchased from ATCC (United States). Human CB-MNC, and human serum albumin were provided by Qilu Stem Cell Engineering Co., Ltd. (Shandong, China). Sodium hyaluronate (Mn of 200 kDa) is provided by Xi'an Baichuan Biotechnology Co., Ltd. NOCC (deacetylation degree of 98%, Mn of 180 kDa) is provided by Shanghai Yuwei Biotechnology Development Co., Ltd. Sodium periodate (99.5% of purity), ethylene glycol (98% of purity) and phosphate buffer saline (PBS) were obtained from Shanghai Macklin Biochemical Technology Co., Ltd. Dulbecco's modified Eagle medium (DMEM), fetal bovine serum (FBS) and other reagents were purchased from Thermo Fisher Scientific. Physiological saline was supplied by Sichuan Keren Pharmaceutical Co. All solvents were of analytical grade and used as received.

Male Kunming mice (8 weeks old) were purchased from Jinan Pengyue Experimental Animal Breeding Co., Ltd (China). Animal care procedures complied with the requirements of the Guide for the Care and Use of Laboratory Animals. All animal experiments were approved by the Animal Experimentation Ethics Committee of

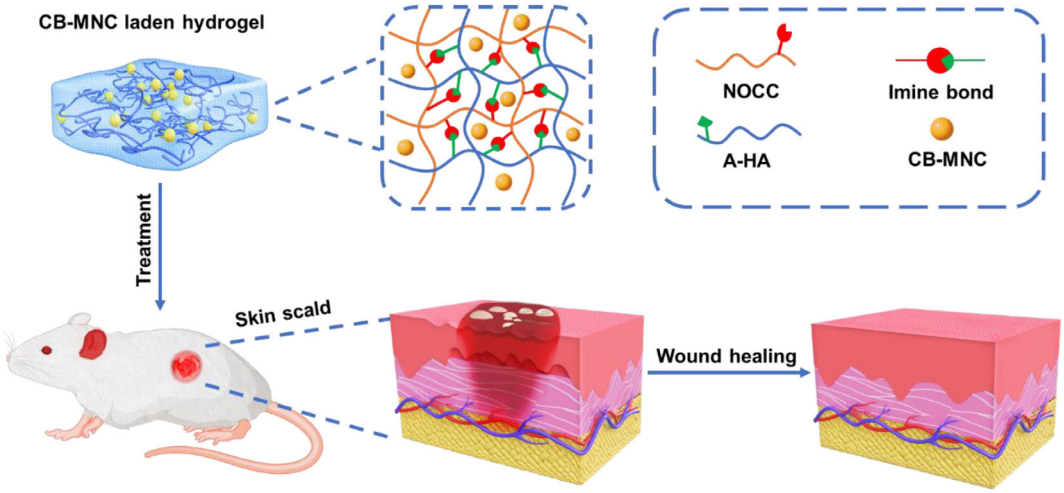

SCHEME 1 Schematic diagram of NOCC/A-HA hydrogel combined with cord blood mononuclear cells (CB-MNC) for the treatment of scald in mice.

Qingdao University of Science and Technology (approval number: 2017-1).

2.2 | Synthesis of A-HA and NOCC/A-HA hydrogels

One gram of HA was dissolved in 100 mL of deionized water, yielding a homogeneous solution at a concentration of 10 mg/mL. Five milliliters of 2.5 mM sodium periodate were then added. The reaction proceeded at room temperature in the dark for 24 h. One milliliter of ethylene glycol was then added, and stirred for 1 h to quench the remaining sodium periodate. The solution was dialyzed (MWCO 10 kDa) for 3 days against deionized water, and finally freeze-dried to yield a dry product.

NOCC and A-HA were separately dissolved in pH 7.4 PBS at a concentration of 30 mg/mL. NOCC and A-HA solutions were mixed at different volume ratios. Gelation then proceeded at 37°C for 24 h to yield hydrogels, namely $Gel_{2\text{-}1}$, $Gel_{4\text{-}1}$, $Gel_{6\text{-}1}$, and $Gel_{8\text{-}1}$ corresponding to NOCC/A-HA volume ratios of 2/1, 4/1, 6/1, and 8/1.

2.3 | Characterization

Fourier transform infrared (FT-IR) spectroscopy was performed on a TENSOR 27 from BRUKER (Germany), in the wavenumber range of 4000–500 cm^{-1} at room temperature. The samples were prepared by using the KBr pellet method.

Proton nuclear magnetic resonance (^1H NMR) spectra were registered by using Bruker spectrometer at 500 MHz at 25°C. Measurements were made using deuterium water (D_2O) as solvent and tetramethylsilane (TMS) as an internal standard.

The structure of hydrogel was examined by using VEGA3 scanning electron microscope (SEM, Tescan, Czech Republic) operating at an accelerating voltage of 20 kV. Freeze-dried hydrogel was quenched in liquid nitrogen and carefully broken. The cross-section was gold-coated before observation.

The rheological properties of NOCC/A-HA hydrogels were determined by using ARES-G2 rotary rheometer (TA, United States). Hydrogels prepared in PBS with a diameter of 25 mm and a thickness of 3 mm were placed on a flat plate of 25 mm. Changes in storage modulus (G') and loss modulus (G'') were followed as a function of time, strain and frequency at 25°C.

2.4 | Swelling and self-healing of hydrogels

Freeze dried samples were weighed and immersed in pH 7.4 PBS at 37°C. At present time intervals, the samples were withdrawn, wiped with filter paper to remove surface water, and weighed. The swollen samples were lyophilized and weighed again. The swelling ratio was calculated by using the following equation:

$$\text{Swelling}\,(\%) = \frac{(M_s - M_d)}{M_d} \times 100 \quad (1)$$

where M_s the wet mass of the swollen hydrogel, and M_d the remaining dry mass. Triplicate experiments are made for each data point.

The self-healing behavior of the hydrogel was assessed by reintegration test of split pieces. The hydrogels were stained red with neutral red, incubated at 37°C for 24 h, and then cut into two pieces. The pieces were immediately put together at 37°C to examine the reintegration.

2.5 | Biocompatibility

2.5.1 | MTT assay

The 3-(-4,5-Dimethylthiazol-2-yl)-2,5-diphenyltetrazolium bromide (MTT) assay was used to evaluate the cytotoxicity of hydrogels. Lyophilized hydrogels (7.5 mg) were immersed in 5 mL DMEM containing 10% fetal bovine serum, and incubated at 37°C for 24 h. One hundred microliters of L929 cells were seeded in a 96-well cell culture plate at a density of 1×10^4 cells/well for 24 h. One hundred microliters of hydrogel extract was then added to replace the original culture medium, and incubated for 24, 48, and 72 h. Pure culture medium was taken as negative control, and culture medium containing 0.5% phenol as positive control. Cell viability was determined from the OD values of the test sample and the negative control according to the following equation:

$$\text{Cell viability}\,(\%) = \frac{\text{OD}_{\text{test sample}}}{\text{OD}_{\text{negative control}}} \times 100 \qquad (2)$$

2.5.2 | Zebrafish embryotoxicity test

Adult zebrafish embryos were collected and transferred to individual wells of a 96-well plate. Lyophilized hydrogel (7.5 mg) was soaked in 5 mL of medium and incubated at 37°C for 24 h. The embryos were then co-cultured with the hydrogel extract. The medium containing acetone served as a positive control, and the medium served as a negative control. Mortality and morphological deformities were assessed after 96 h.

2.6 | Viability of CB-MNC in hydrogels

After sterilization by ultraviolet radiation, NOCC and A-HA were dissolved in pH 7.4 PBS at a concentration of 60 and 30 mg/mL, respectively. The CB-MNC cell density was adjusted to 1×10^7 cells/mL. The cell suspension was mixed with A-HA solution in equal volumes in a 6-well plate, followed by addition of NOCC solution. Live/dead cells were stained by using AO/PI staining, and observed under a fluorescent microscope. Cell viability was recorded up to 21 days.[39] Image J software (live/dead cell image analysis) was used to quantify the number of surviving cells. Similarly, cell laden hydrogels were prepared in DMEM and saline containing 1% human albumin, and cell viability was recorded up to 21 days. For the sake of comparison, CB-MNC at a density of 1×10^7 cells/mL were cultured in DMEM and saline containing 1% human albumin, and cell viability was recorded up to 3 days.

2.7 | Anti-adhesion of NOCC/A-HA hydrogels

NOCC and A-HA solutions were mixed in a 6-well plate, and incubated 24 h at 37°C to yield a hydrogel. L929 cells in suspension were then added on the surface of hydrogel. After 24 h incubation at 37°C, live/dead cells were stained using AO/PI staining, and cell morphology was observed with an inverted fluorescence microscope.

2.8 | Mouse scald model

Fifteen healthy mice were randomly divided into three groups of five mice each: Control group (without treatment), Gel group (treatment with hydrogel), and Gel + CB-MNC group (treatment with cell laden hydrogel). The back of the mice was shaved. After anesthesia, the mice were scalded with hot water at 90°C for 10 s on the back avoiding the spinal cord side, yielding a deep second-degree scald. The scalds were treated with neat hydrogel or cell laden hydrogel. Scald healing was examined after 0, 1, 7, 14, and 21 days. The wound area was recorded with a camera, and the image processing software (Image J) was used to assess the wound closure rate. Then the wound tissue and surrounding normal tissue were excised. The excised skin tissues were fixed in formaldehyde solution, dehydrated, and paraffin-embedded. Pathological sections were examined with hematoxylin and eosin (H&E) staining to assess cell expression, capillary expression, and epidermal healing. All animal experiments were performed in compliance with the guidelines of the National Research Council's Guide for the Care and Use of Laboratory Animals.

3 | RESULTS AND DISCUSSION

3.1 | Characterization of polysaccharide derivatives

^{1}H NMR was used to characterize NOCC and A-HA. As shown in Figure 1a, NOCC exhibits characteristic peaks at 3.1 ppm (H-2), at 3.5–4.0 ppm (H-3 to H-6) and a small

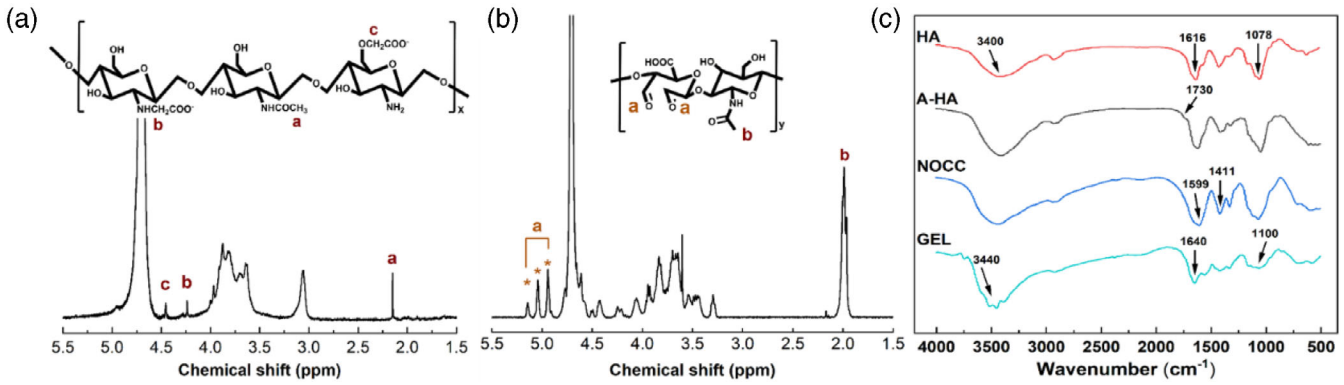

FIGURE 1 Proton nuclear magnetic resonance (^{1}H NMR) spectrum of NOCC (a); ^{1}H NMR spectrum of A-HA (b); Fourier transform infrared (FTIR) spectra of HA, A-HA, NOCC, and NOCC/HA hydrogel (c).

single peak at 2.2 ppm assigned to the methyl protons of *N*-acetyl groups. Two small peaks are detected at 4.2 and 4.4 ppm which are assigned to the —CH_2COO— protons at the *N*-position of C_2 and the *O*-position of C_6 of NOCC, respectively, in agreement with the carboxymethyl substitution on the amino group (*N*-position) and primary hydroxyl group (*O*-position).[40,41]

The ^{1}H NMR spectrum of A-HA is shown in Figure 1b. Broad signals between 3.2 and 3.7 ppm correspond to various protons in the sugar ring. The methyl protons of the *N*-acetyl group of HA are detected at 2.0 ppm. Signals observed at 4.9, 5.0, and 5.1 ppm are assigned to aldehyde groups. The degree of oxidation is quantified by comparing the integrals of the aldehydes and the methyl of the *N*-acetyl group in the HA backbone. The obtained degree of oxidation is 56%.

NOCC/A-HA hydrogels were prepared by cross-linking via Schiff base reaction between the amino groups of NOCC and the aldehyde groups of A-HA. The FTIR spectra of HA, A-HA, NOCC, and $Gel_{4\text{-}1}$ are shown in Figure 1c. HA presents characteristic peaks at 3400, 1616, and 1078 cm^{-1} which are assigned to the —OH absorption, the antisymmetric stretching vibration of —COOH, and the stretching absorption of C—O bonds, respectively. The spectrum of A-HA is very similar to that of HA, excepting the appearance of a small band at 1730 cm^{-1} which belongs to the aldehyde groups. In the spectrum of NOCC, the bands at 1599 and 1411 cm^{-1} are assigned to asymmetric and symmetric stretching of carboxylate groups (—COO^-), respectively.[42] The spectrum of $Gel_{4\text{-}1}$ shows all the characteristic bands of NOCC and A-HA. The bands at 3200–3500 and 1100 cm^{-1} are attributed to free OH and NH_2 groups, and CO stretching, respectively. Interestingly, the small band at 1730 cm^{-1} of aldehyde groups disappears, and the band at 1640 cm^{-1} belongs to both carboxylate and imine groups, in agreement with formation of NOCC/A-HA hydrogel by imine bond formation between the amino groups of NOCC and the aldehyde groups of A-HA.[20,22]

3.2 | Characterization of hydrogels

SEM was used to qualitatively assess the microstructure of lyophilized hydrogels (Figure 2a–d). The different hydrogels exhibit a porous structure with interconnected pores. $Gel_{2\text{-}1}$ seems to have larger pore size (up to 300 μm) as compared to the others. $Gel_{4\text{-}1}$ exhibits the most uniform porous structure with pore size ranging from 50 to 200 μm, whereas $Gel_{6\text{-}1}$ and $Gel_{8\text{-}1}$ present a less regular porous structure. The interpenetration and connectivity of pores of hydrogels are of major importance as they allow the diffusion of nutrients, gases, and metabolites, and support the survival and growth of cells.

3.3 | Rheological properties of hydrogels

The gelation process of mixed NOCC and A-HA aqueous solutions was monitored in situ on the rheometer plate by following changes of the storage modulus (G') and loss modulus (G'') as a function of time at 25°C. For all samples, the storage modulus is initially lower than the loss modulus (Figure 3a), which means that the initial mixture is a liquid. Both G' and G'' increase with gelation time, G' increasing much faster than G''. The intersection between G' and G'' indicates sol–gel transition. The gelation time decreases from 89 s for $Gel_{2\text{-}1}$ to 58 s for $Gel_{4\text{-}1}$, and then increases to 107 s for $Gel_{6\text{-}1}$ and to 177 s for $Gel_{8\text{-}1}$. In fact, gelation occurs through cross-linking or formation of imine bonds, and therefore depends on the ratio between the amino groups of NOCC and the aldehyde groups of A-HA. The cross-linking is not complete for $Gel_{2\text{-}1}$ probably due to lack of amino

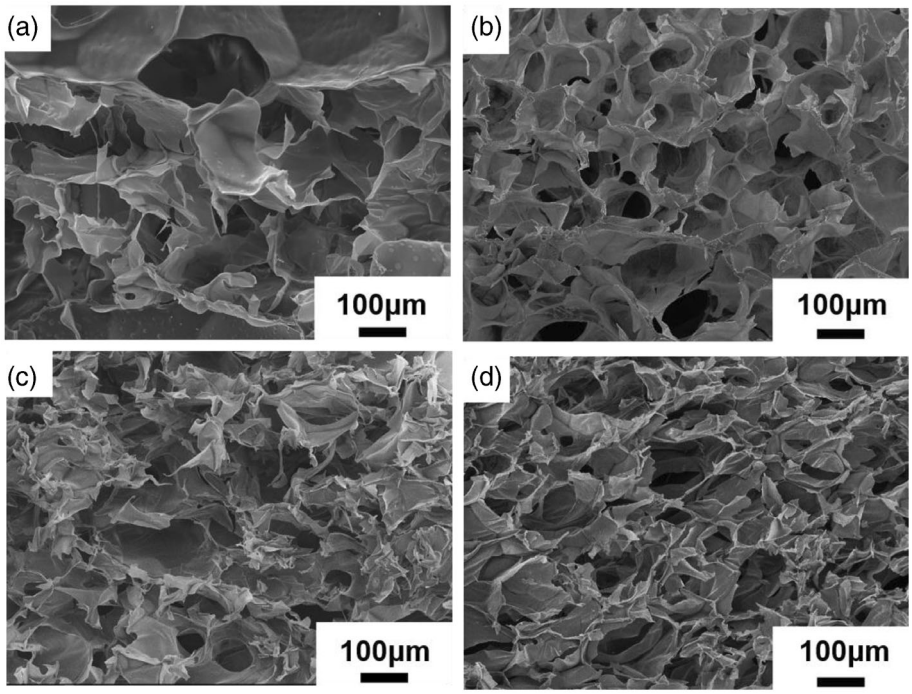

FIGURE 2 Scanning electron microscopy (SEM) images of $Gel_{2\text{-}1}$ (a); $Gel_{4\text{-}1}$ (b); $Gel_{6\text{-}1}$ (c); $Gel_{8\text{-}1}$ (d).

groups. As the NOCC/A-HA ratio increases to 4/1, gelation is improved as more amino groups are available for Schiff base reaction. However, as the ratio further increases to 6/1 and 8/1, the gelation becomes longer due to fewer aldehyde groups available for imine bond formation.

Modulus changes of formed hydrogels are also monitored as a function of frequency at fixed strain (1%) or as a function of strain at fixed frequency (1 Hz), respectively. At a fixed strain of 1%, G' of all samples remains almost stable in the frequency range of 0.1–10 Hz expect $Gel_{2\text{-}1}$ whose G' slightly increases. Beyond 10 Hz, G' rapidly increases. In all cases, G' is much higher than G'' (Figure 3b). In the strain sweep, both G' and G'' remain almost stable in the strain range from 0.01% to 2% (Figure 3c). G' is 691, 995, 883, and 821 Pa at 1% strain for $Gel_{2\text{-}1}$, $Gel_{4\text{-}1}$, $Gel_{6\text{-}1}$, and $Gel_{8\text{-}1}$, respectively, suggesting that $Gel_{4\text{-}1}$ has an optimal crosslinking network, in agreement with gelation time data. G' begins to decrease and G'' to increase beyond a strain of 2% for $Gel_{2\text{-}1}$ and $Gel_{4\text{-}1}$, indicating that the structure of hydrogels is affected. Nevertheless, $Gel_{6\text{-}1}$ and $Gel_{8\text{-}1}$ seem to be more stable as no modulus changes are observed until a strain of 10%.

3.4 | Swelling of hydrogels

The swelling properties of hydrogels are of great importance for biomedical applications as cell carrier or scaffold. Figure 3d shows the equilibrium swelling ratios of different hydrogels after 24 h immersion in PBS at 37°C. The swelling rate of $Gel_{2\text{-}1}$, $Gel_{4\text{-}1}$, $Gel_{6\text{-}1}$, and $Gel_{8\text{-}1}$ is 284%, 427%, 332%, and 217%, respectively. $Gel_{4\text{-}1}$ presents the highest swelling rate due to the uniform porous structure which favors water absorption and water retention, in agreement with SEM results.

Rheological and swelling experiments suggest that $Gel_{4\text{-}1}$ presents the best overall properties, and is thus selected for further investigations.

3.5 | Self-healing of hydrogels

The self-healing properties of hydrogels were assessed by reintegration test. A dyed red hydrogel and a transparent hydrogel were cut into two pieces, and the cut pieces were put together at 37°C. The samples were totally integrated after 2 h. The healed hydrogel can be peeled off and support its own weight (Figure 4a). The self-healing capacity of hydrogels can be attributed to the reconstruction of reversible imine bond crosslinking, and migration of components or constituent exchanges between cut pieces.[20,43] Rheological experiments were performed on self-healed hydrogels. As shown in Figure 4b, the self-healed $Gel_{4\text{-}1}$ presents G' and G'' values very close to those of the original hydrogel, thus confirming the outstanding self-healing capacity. The self-healing of hydrogel enables to ensure its structural integrity when applied to wounds in clinical treatment, thus facilitating the repair and treatment of complex wounds.

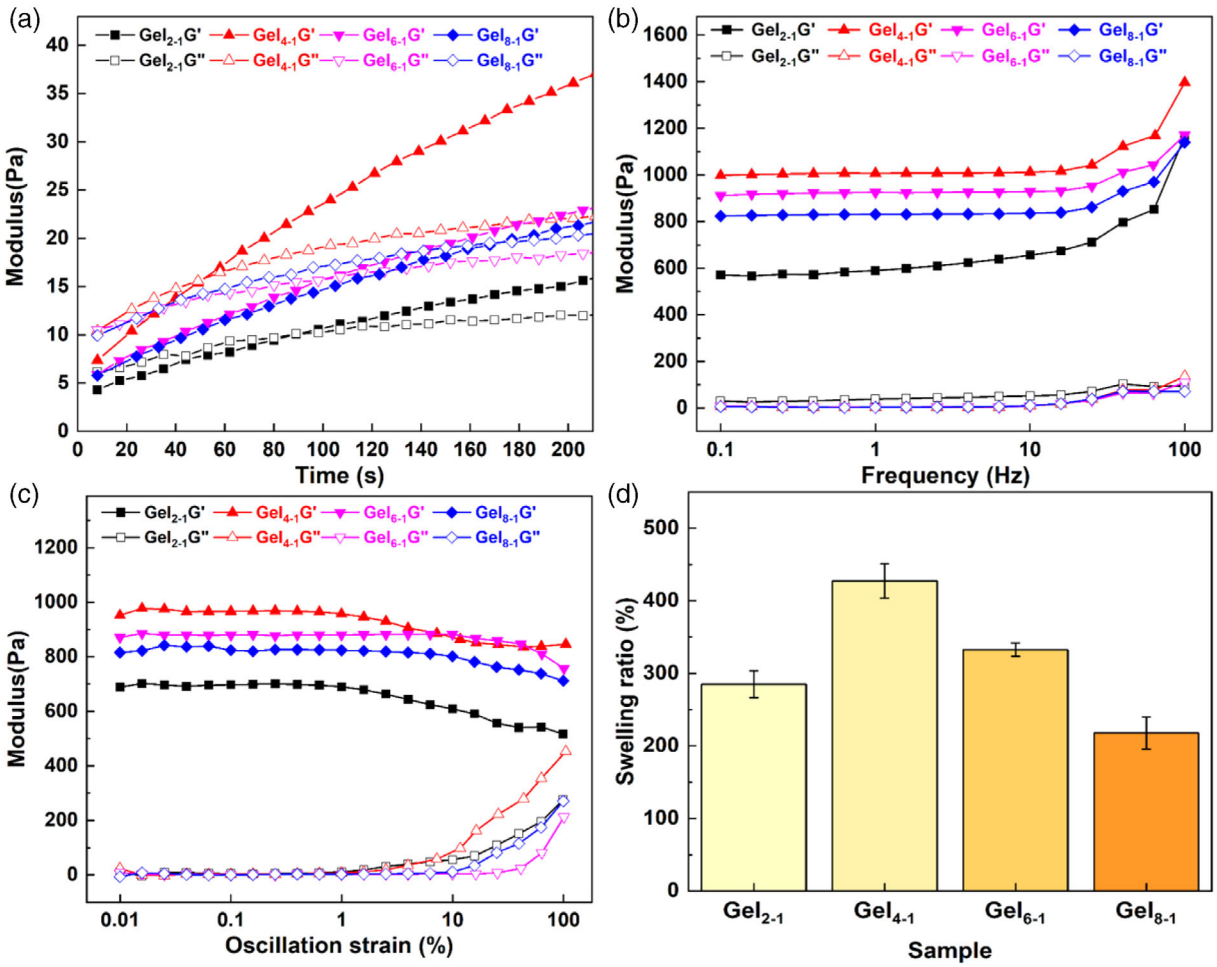

FIGURE 3 Rheological properties of NOCC/A-HA hydrogels: G' and G'' changes as a function of gelation time at 25°C (a); G' and G'' changes as a function of frequency at 25°C and at 1% strain (b); G' and G'' changes as a function of strain at 25°C and at 1 Hz (c); Swelling ratios of hydrogels after 24 h immersion in pH = 7.4 PBS at 37°C (d). ($n = 3$).

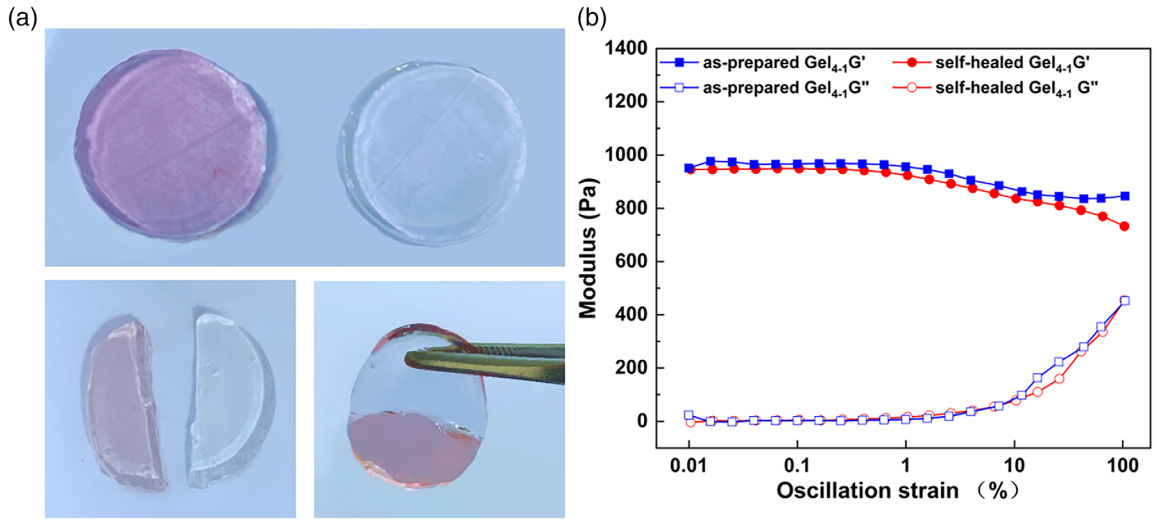

FIGURE 4 Self-healing test of NOCC/A-HA hydrogel by reintegration of cut pieces (a); G' and G'' changes as a function of strain of as-prepared hydrogel and self-healed hydrogel at 25°C (b)

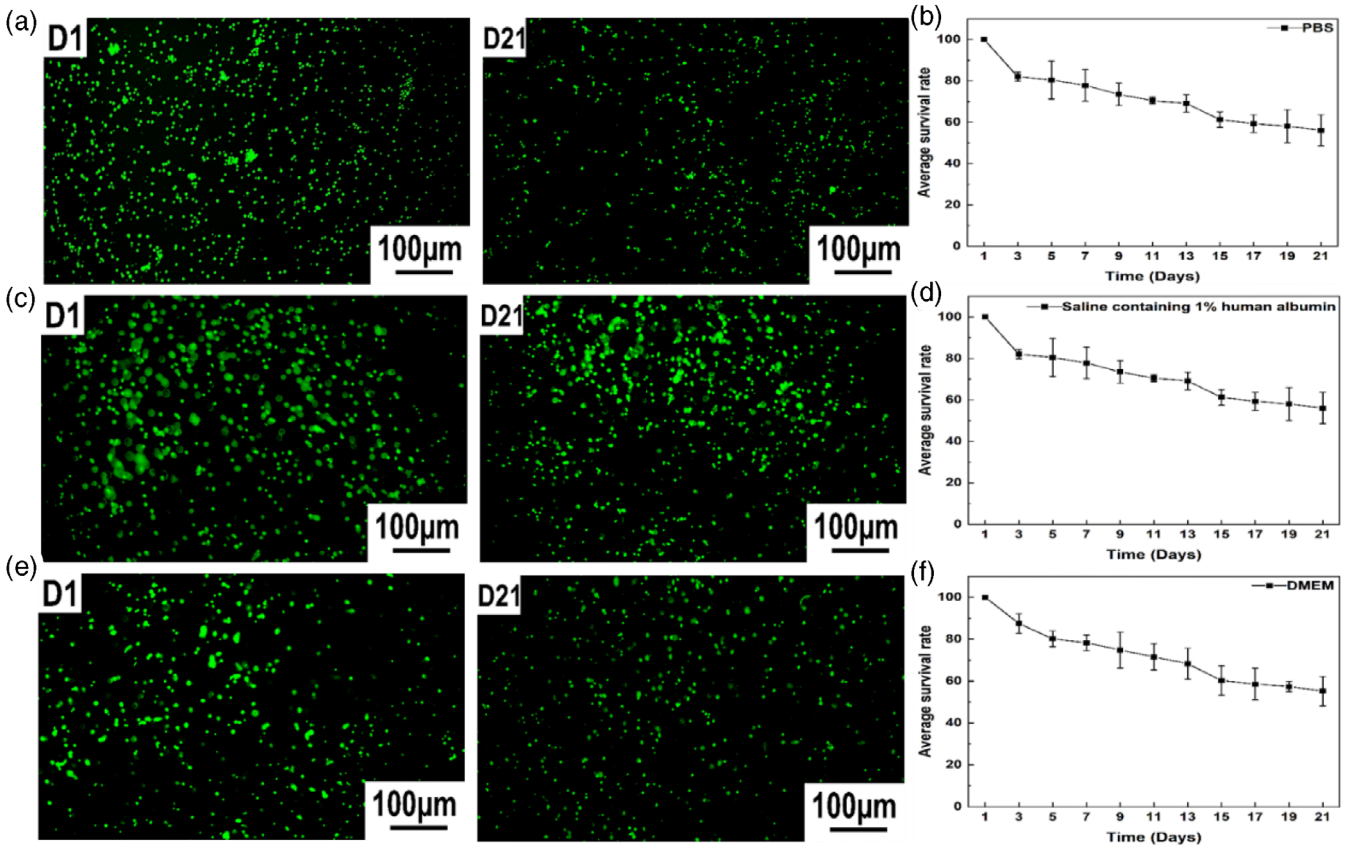

FIGURE 5 Images of CB-MNC after 1 and 21 days culture in hydrogels prepared in PBS (a), in saline containing 1% human albumin (c), and in DMEM (e); Average survival rate of CB-MNC in hydrogels prepared in PBS (b), in saline containing 1% human albumin (d), and in DMEM (f). ($n = 3$).

3.6 | Biocompatibility of hydrogels

The biocompatibility of NOCC/A-HA hydrogel was evaluated by MTT assay and Zebrafish embryotoxicity test. Figure S1 shows the viability of L929 cells after co-culture with extracts of different hydrogels for 24, 48, and 72 h. The cell viability of the positive control was very low, decreasing from 26% at 24 h to 14% at 72 h. In contrast, the cell viability were above 79% throughout the culture period up to 72 h for all samples. Therefore, the various NOCC/A-HA hydrogels with different compositions are not toxic to L929 mouse fibroblasts, and can be safely applied on the wound surface in clinical applications in accordance with the ISO 10993.

Zebrafish is increasingly used as a vertebrate animal model for in vivo drug discovery and for assessing chemicals toxicity. In fact, zebrafish and mammals are similar in their physiology, development, metabolism and pathways. Zebrafish responses to toxic substances are thus highly predictive of mammalian responses. Toxicity and safety assessments using zebrafish have been accepted by the FDA and European agency for the evaluation of medicinal products (EMEA) for investigational new drug approval. In the present work, zebrafish embryotoxicity test was performed to further confirm the non-toxicity of hydrogels. After 96 h co-culture with $Gel_{4\text{-}1}$ extract, the embryos developed normally (Figure S2a). In contrast, embryos in the positive control showed malformation with enlarged yolk sacs (Figure S2b), malformation of pericardial edema and abnormal caudal fins (Figure S2c), and embryonic death (Figure S2d). These findings indicate that hydrogels are not harmful to embryo development, and are not embryotoxic or teratogenic.

3.7 | Cell viability in hydrogels

CB-MNC were loaded in hydrogels prepared in PBS at a concentration of 1×10^7 cells/mL, and cultured up to 21 days at 37°C to evaluate the cytocompatibility. All cells were stained by live/dead assay with AO/PI kit. As shown in Figure 5a, the cells appeared round-shaped, and were uniformly distributed in the hydrogel up to 21 days culture. The cell survival rate slowly decreased with culture time, reaching $51 \pm 4\%$ % at day 21 (Figure 5b).

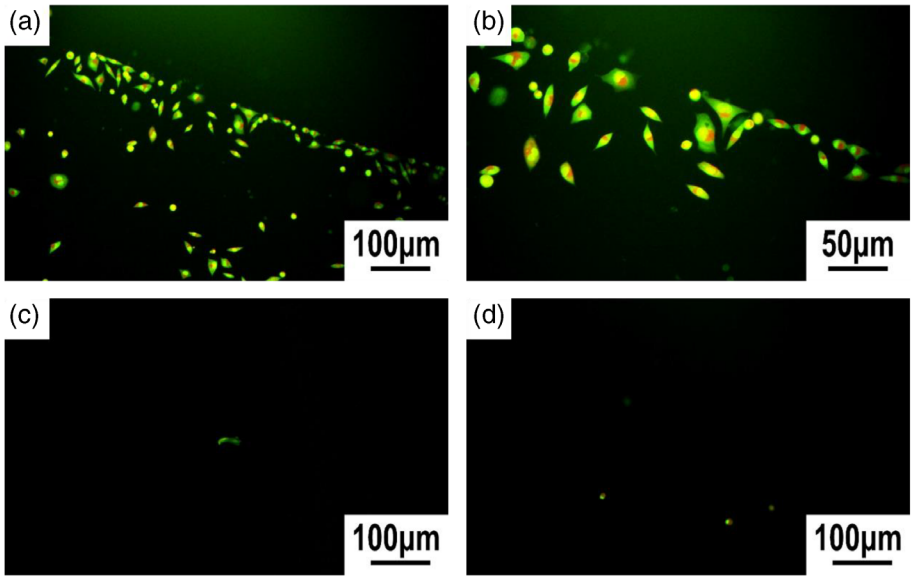

FIGURE 6 L929 cell attachment at the junction of hydrogel and culture dish (a); Magnified view of L929 cells at the boundary of hydrogel (b); L929 cells on the surface of hydrogel (c, d). ($n = 3$).

CB-MNC were also cultured in hydrogels prepared in saline containing 1% human albumin (Figure 5c) and in DMEM (Figure 5e). The cell morphology appeared very similar to that in hydrogels prepared in PBS (Figure 5a). The survival rate was 56 ± 8% and 55 ± 7% at day 21 for cells cultured in hydrogels prepared in saline (Figure 5d) and in DMEM (Figure 5f), respectively. Therefore, there is no significant difference in the average survival rates of CB-MNC in hydrogels prepared in PBS, in saline and in DMEM, suggesting that the two media containing nutrients have no significant effect on cell survival.

In order to demonstrate the beneficial effect of hydrogels on cell survival, CB-MNCs were cultured in liquid media, that is, DMEM and saline containing 1% human albumin. As shown in Figure S3a,b, the cell survival rate rapidly decreased to 47% after 12 h culture in DMEM, and all cells were apoptotic after 96 h. In the case of cell culture in saline containing 1% human albumin (Figure S3c,d), the cell survival rate decreased to 55% after 12 h, and all cells were apoptotic after 96 h. Therefore, although both media can provide nutrients for cell growth, cells cannot survive due to the lack of a good living environment. It is thus supposed that the hydrogel network could be coupled with adhesive ligands for cell attachment, providing an environment which is beneficial to cell growth.

3.8 | Cell invasion test

Under the stimulation of trauma and other factors, fibroblasts can be re-transformed into immature fibroblasts and participate in the repair of tissue damage. During the repair process, contact between wounds can cause tissue adhesion.[44,45] The ability of the hydrogel to prevent tissue adhesion was verified by fibroblast invasion test.

L929 cells were co-cultured with NOCC/A-HA hydrogel to assess cell adhesion to the hydrogel surface, and to figure out whether hydrogels could prevent fibroblast invasion. During co-culture, L929 cells were stretched in a shuttle shape against the bottom at the edge of the hydrogel (Figure 6a), and the stretched pattern of cells could be clearly observed upon magnification (Figure 6b). In contrast, only a few cells were present on the surface of the hydrogel (Figure 6c,d). Moreover, the cells appeared spherical in shape without agglomeration. This suggests that the surface of NOCC/A-HA hydrogel is not favorable for the attachment of fibroblasts probably due to the highly hydrophilic nature of the hydrogel surface. Taking into account that fibroblasts are common cells in connective tissues, it is concluded that NOCC/A-HA hydrogel can prevent tissue adhesion that occurs when wound tissue was damaged, and thus improve the efficiency of wound healing.

3.9 | Mouse scalding model

NOCC/A-HA hydrogel containing CB-MNC was developed to evaluate its potential in treating burns or scalds and preventing scarring. A deep second-degree scald model was established on the back of mice, and treated with the hydrogel (Gel group) and the hydrogel containing CB-MNC (Gel + CB-MNC group). The untreated mice group was taken as control. In the control group, the scalds healed slowly, and scabs appeared on the wound surface from the third to seventh day (Figure 7a). The color of the epidermis deepened. A large scar was

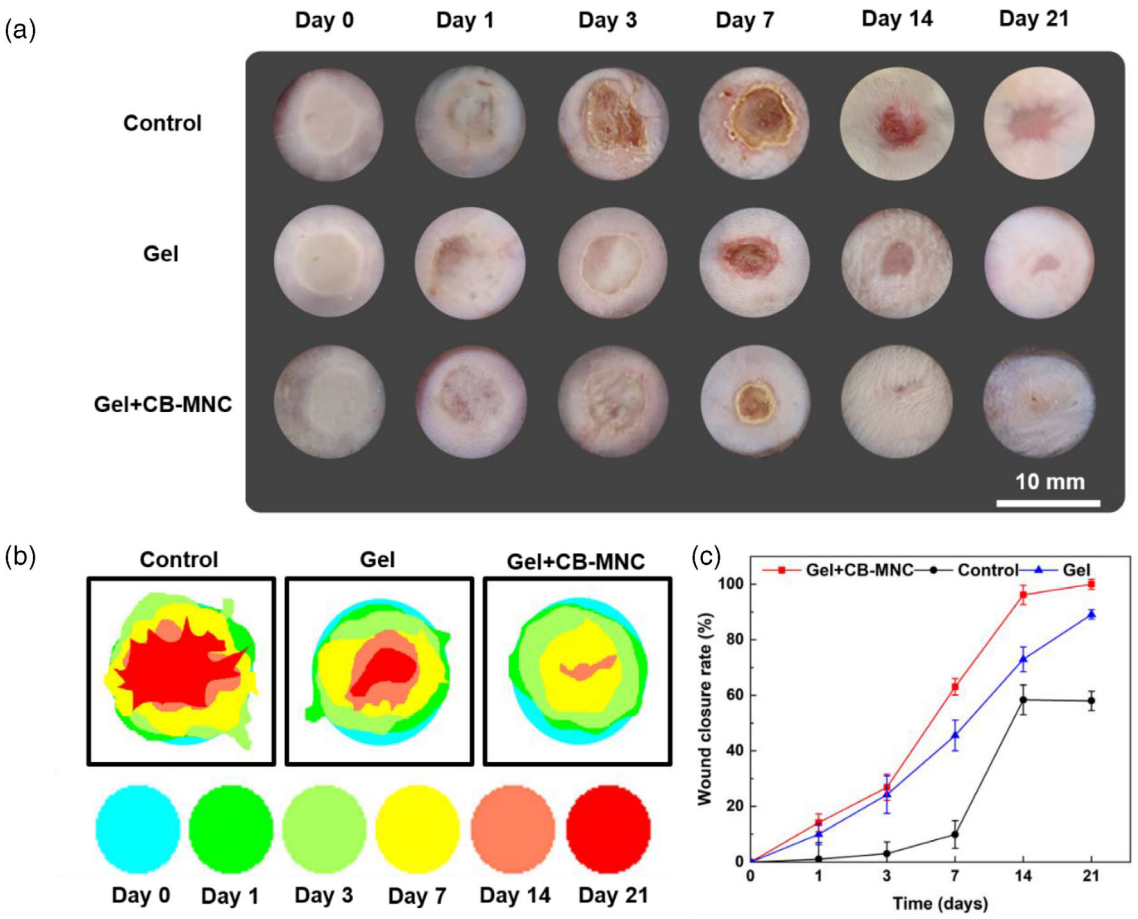

FIGURE 7 Representative photographs of wound healing of the three groups during 21 days (a); relative wound area of mice after different treatment times (b); wound closure rates of the three groups during 21 days treatment (c). ($n = 5$). [Color figure can be viewed at wileyonlinelibrary.com]

observed after 21 days healing. The Gel group showed faster healing, and the scar formed after healing appeared smaller than that of the control group. Gel + CB-MNC group healed faster as compared to the two other groups, with regular shrinkage of the wound area over time. Almost no scar was observed after healing. This may be attributed to the fact that hydrogel prevented dehydration of the wound surface, and that CB-MNC in the hydrogel enhanced epithelialization.

Wound healing area graphics and plots are shown in Figure 7b,c, respectively. The results showed that compared to the control group, NOCC/A-HA hydrogel improved scald healing due to the prevention of dehydration, but did not prevent scarring. In contrast, CB-MNC loaded hydrogel can not only promote scald healing, but also greatly reduce post-healing scarring.

Cell infiltration, neovascularization, and epidermal regeneration at different times were examined using H&E staining to further analyze the wound healing efficiency (Figure 8). At the first day after scalding, it was observed that the nuclei of the epidermal cells of the scalded skin were pyknosis, the deep layer of the dermis was damaged, collagen fibers were fused, and hair follicles remained. These observations well agreed with the criteria for deep second-degree burns. On the seventh day, inflammatory cells in the control group were obviously infiltrated, showing incomplete keratinization. In the Gel group, the epidermis was regenerated, the dermis was loosely arranged, and the inflammation was moderately infiltrated. In the Gel + CB-MNC group, the epidermis was regenerated, the edema of the acanthoid layer was reduced, and the inflammatory infiltration was reduced.[46,47] On the 14th day, the appearance of skin appendages, increased angiogenesis and sustained epithelialization were observed in the Gel + CB-MNC group; the Gel group showed less angiogenesis and less inflammatory infiltration; and the control group showed incomplete keratosis and reduced epidermal regeneration. On the 21st day, the epidermis and dermis in the Gel + CB-MNC group recovered well, and complete epithelialization and vascularization were observed without epidermal thickening. The control group showed complete

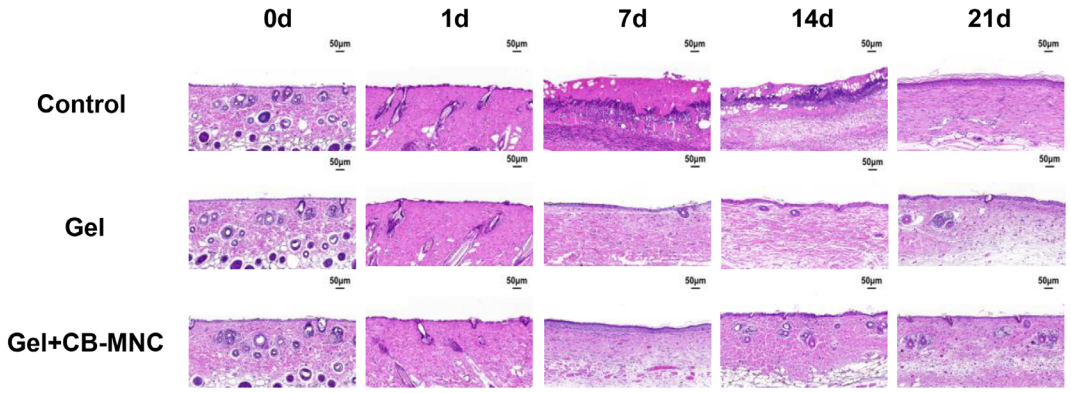

FIGURE 8 Histological studies with hematoxylin and eosin (H&E) staining of the skin at different times up to 21 days showing the process of skin tissue regeneration of the three groups.

epidermal epithelialization with dermal fibrosis. And the Gel group showed nearly complete epithelialization, but poor differentiation of the layers of the new epidermis.

4 | CONCLUSIONS

Dynamic hydrogels were prepared by Schiff base reaction between the amino groups of NOCC and aldehyde ones of A-HA, and used to encapsulate CB-MNCs for scald treatment. NOCC/A-HA hydrogels present outstanding rheological and swelling properties, and self-healing performance. The biocompatibility of hydrogels was evidenced by MTT assay and zebrafish embryonic toxicity test. Human umbilical CB-MNC loaded in the hydrogel showed high survival rate above 50% after 21 days culture. A mouse scald model was realized to evaluate the potential of cell laden hydrogel in wound healing. Compared to the control group and hydrogel group, the cell laden hydrogel group exhibits faster epidermal regeneration, reduced inflammation and more neovascularization, suggesting that CB-MNC is beneficial to epithelialization. Therefore, it is concluded that CB-MNC loaded NOCC/A-HA hydrogel could be promising for applications in the treatment of burns or scalds.

AUTHOR CONTRIBUTIONS

Shaowen Kong: Data curation (lead); investigation (lead); writing – original draft (lead). **Jie Song:** Data curation (supporting); methodology (equal). **Yuandou Wang:** Investigation (supporting). **Shuxin Wang:** Methodology (supporting). **Feng Su:** Conception; supervision. **Suming Li:** Supervision; revision.

ACKNOWLEDGMENTS

The work was financially supported by the Shandong Provincial Natural Science Foundation (ZR2021ME208) and Wanhua Chemical Group (project No 20213702032181).

CONFLICT OF INTEREST STATEMENT

The authors declare no conflicts of interest. This research did not receive any specific grant from funding agencies in the public, commercial, or not-for-profit sectors.

DATA AVAILABILITY STATEMENT

The data that support the findings of this study are available from the corresponding author upon reasonable request.

ORCID

Suming Li https://orcid.org/0000-0002-3345-1479

REFERENCES

[1] M. Aragona, S. Dekoninck, S. Rulands, S. Lenglez, G. Mascré, B. D. Simons, C. Blanpain, *Nat. Commun.* **2017**, *8*, 14684.
[2] M. I. AlJasser, G. de Gannes, *J. Am. Acad. Dermatol.* **2021**, *84*, e83.
[3] I. Spronk, S. Polinder, J. A. Haagsma, M. Nieuwenhuis, A. Pijpe, C. H. van der Vlies, E. Middelkoop, M. E. van Baar, *Wound Repair Regen.* **2019**, *27*, 406.
[4] K. Skórkowska-Telichowska, M. Czemplik, A. Kulma, J. Szopa, *J. Am. Acad. Dermatol.* **2013**, *68*, e117.
[5] V. L. Tsang, S. N. Bhatia, *Adv. Drug Deliv. Rev.* **2004**, *56*, 1635.
[6] J. Wasiak, H. Cleland, F. Campbell, A. Spinks, *Cochrane Database Syst. Rev.* **2013**, *2013*, Cd002106.
[7] V. S. Raghuwanshi, G. Garnier, *Adv. Colloid Interface Sci.* **2019**, *274*, 102044.
[8] O. Qianqian, K. Songzhi, H. Yongmei, J. Xianghong, L. Sidong, L. Puwang, L. Hui, *Int. J. Biol. Macromol.* **2021**, *181*, 369.
[9] B. Grigoryan, S. J. Paulsen, D. C. Corbett, D. W. Sazer, C. L. Fortin, A. J. Zaita, P. T. Greenfield, N. J. Calafat, J. P. Gounley, A. H. Ta, F. Johansson, A. Randles, J. E. Rosenkrantz, J. D. Louis-Rosenberg, P. A. Galie, K. R. Stevens, J. S. Miller, *Science* **2019**, *364*, 458.
[10] Y. Yang, A. Campbell Ritchie, N. M. Everitt, *Mater. Sci. Eng. C Mater. Biol. Appl.* **2021**, *121*, 111846.
[11] Q. Huang, Y. Zou, M. C. Arno, S. Chen, T. Wang, J. Gao, A. P. Dove, J. Du, *Chem. Soc. Rev.* **2017**, *46*, 6255.

[12] J. da Silva, A. Lucas, E. Quadro Oreste, H. Leão Gouveia Costa, H. Martín López, C. Dias Medeiros Saad, C. Prentice, *Food Chem.* **2021**, *343*, 128550.
[13] W. Wang, C. Xue, X. Mao, *Int. J. Biol. Macromol.* **2020**, *164*, 4532.
[14] X. Cao, L. Sun, Z. Luo, X. Lin, Y. Zhao, *Eng. Regen.* **2023**, *4*, 28.
[15] C. Cui, S. Sun, S. Wu, S. Chen, J. Ma, F. Zhou, *Eng. Regen.* **2021**, *2*, 82.
[16] R. C. Cheung, T. B. Ng, J. H. Wong, W. Y. Chan, *Mar. Drugs* **2015**, *13*, 5156.
[17] N. A. Negm, H. H. H. Hefni, A. A. A. Abd-Elaal, E. A. Badr, M. T. H. Abou Kana, *Int. J. Biol. Macromol.* **2020**, *152*, 681.
[18] L. Li, N. Wang, X. Jin, R. Deng, S. Nie, L. Sun, Q. Wu, Y. Wei, C. Gong, *Biomaterials* **2014**, *35*, 3903.
[19] H. Li, F. Cheng, X. Wei, X. Yi, S. Tang, Z. Wang, Y. S. Zhang, J. He, Y. Huang, *Mater. Sci. Eng. C Mater. Biol. Appl.* **2021**, *118*, 111324.
[20] R. Yu, Y. Zhang, M. Barboiu, M. Maumus, D. Noël, C. Jorgensen, S. Li, *Carbohydr. Polym.* **2020**, *244*, 116471.
[21] R. Yu, E. Petit, M. Barboiu, S. Li, W. Sun, C. Chen, *Mater. Sci. Eng. C Mater. Biol. Appl.* **2021**, *127*, 112210.
[22] R. Yu, L. Cornette de Saint-Cyr, L. Soussan, M. Barboiu, S. Li, *Int. J. Biol. Macromol.* **2021**, *167*, 1146.
[23] S. Vasvani, P. Kulkarni, D. Rawtani, *Int. J. Biol. Macromol.* **2020**, *151*, 1012.
[24] M. A. Schwartz, C. S. Chen, *Science* **2013**, *339*, 402.
[25] T. Fan, J. Qin, X. Meng, J. Li, Q. Liu, G. Wang, *Front. Bioeng. Biotechnol.* **2022**, *10*, 1021218.
[26] T. Fan, Y. Zhang, X. Meng, Y. Qu, Y. Wang, Q. Liu, G. Wang, *Colloid Interface Sci. Commun.* **2022**, *51*, 100671.
[27] T. Fan, J. Qin, F. Dong, X. Meng, Y. Li, Y. Wang, Q. Liu, G. Wang, *RSC Adv.* **2022**, *12*, 10711.
[28] A. H. Pandit, N. Mazumdar, S. Ahmad, *Int. J. Biol. Macromol.* **2019**, *137*, 853.
[29] N. T. Nguyen, L. V. Nguyen, N. M. Tran, D. T. Nguyen, T. N. Nguyen, H. A. Tran, N. N. Dang, T. V. Vo, T. H. Nguyen, *Mater. Sci. Eng. C Mater. Biol. Appl.* **2019**, *103*, 109670.
[30] K. Paloczi, *Leukemia* **1999**, *13*, S87.
[31] D. Karamitros, B. Stoilova, Z. Aboukhalil, F. Hamey, A. Reinisch, M. Samitsch, L. Quek, G. Otto, E. Repapi, J. Doondeea, B. Usukhbayar, J. Calvo, S. Taylor, N. Goardon, E. Six, F. Pflumio, C. Porcher, R. Majeti, B. Göttgens, P. Vyas, *Nat. Immunol.* **2018**, *19*, 85.
[32] Y. Shang, H. Guan, F. Zhou, *Front. Cell Dev. Biol.* **2021**, *9*, 570179.
[33] A. Athanassopoulos, G. Tsaknakis, S. E. Newey, A. L. Harris, J. Kean, M. P. Tyler, S. M. Watt, *Burns* **2012**, *38*, 691.
[34] M. Y. Chang, T. T. Huang, C. H. Chen, B. Cheng, S. M. Hwang, P. C. Hsieh, *Stem Cells Transl. Med.* **2016**, *5*, 56.
[35] J. Chen, Y. Chen, X. Du, G. Liu, X. Fei, J. R. Peng, X. Zhang, F. Xiao, X. Wang, X. Yang, Z. Feng, *Front. Cell Dev. Biol.* **2021**, *9*, 679866.
[36] L. Boissel, H. H. Tuncer, M. Betancur, A. Wolfberg, H. Klingemann, *Biol. Blood Marrow Transplant.* **2008**, *14*, 1031.
[37] D. Bist, A. M. Pawde, Amarpal, P. Kinjavdekar, R. Mukherjee, K. P. Singh, M. R. Verma, K. Sharun, A. Kumar, P. K. Dubey, D. Mohan, A. Verma, G. T. Sharma, *Expert Opin. Biol. Ther.* **2021**, *21*, 1655.
[38] Z. Lei, G. Singh, Z. Min, C. Shixuan, K. Xu, X. Pengcheng, W. Xueer, C. Yinghua, Z. Lu, Z. Lin, *Mater. Sci. Eng. C Mater. Biol. Appl.* **2018**, *90*, 159.
[39] H. Park, B. Choi, J. Hu, M. Lee, *Acta Biomater.* **2013**, *9*, 4779.
[40] S. C. Chen, Y. C. Wu, F. L. Mi, Y. H. Lin, L. C. Yu, H. W. Sung, *J. Controlled Release* **2004**, *96*, 285.
[41] J. Liu, J. F. Lu, J. Kan, Y. Q. Tang, C. H. Jin, *Int. J. Biol. Macromol.* **2013**, *62*, 85.
[42] R. Gilli, M. Kacuráková, M. Mathlouthi, L. Navarini, S. Paoletti, *Carbohydr. Res.* **1994**, *263*, 315.
[43] Y. Liang, Z. Li, Y. Huang, R. Yu, B. Guo, *ACS Nano* **2021**, *15*, 7078.
[44] S. Abbasi, S. Sinha, E. Labit, N. L. Rosin, G. Yoon, W. Rahmani, A. Jaffer, N. Sharma, A. Hagner, P. Shah, R. Arora, J. Yoon, A. Islam, A. Uchida, C. K. Chang, J. A. Stratton, R. W. Scott, F. M. V. Rossi, T. M. Underhill, J. Biernaskie, *Cell Stem Cell* **2020**, *27*, 396.
[45] V. Thulabandu, D. Chen, R. P. Atit, *Wiley Interdiscip. Rev. Dev. Biol.* **2018**, *7*, 7.
[46] C. Chen, Y. Wang, D. Zhang, X. Wu, Y. Zhao, L. Shang, J. Ren, Y. Zhao, *Appl. Mater. Today* **2021**, *23*, 101000.
[47] H. Zhang, Z. Zhang, H. Zhang, C. Chen, D. Zhang, Y. Zhao, *ACS Appl. Mater. Interfaces* **2021**, *13*, 18413.

SUPPORTING INFORMATION

Additional supporting information can be found online in the Supporting Information section at the end of this article.